Magnetic Anisotropy of the Antiferromagnetic Ring $[Cr_8F_8Piv_{16}]$

Joris van Slageren,[a] Roberta Sessoli,[a] Dante Gatteschi,*[a] Andrew A. Smith,[b] Madeleine Helliwell,[b] Richard E. P. Winpenny,[b] Andrea Cornia,[c] Anne-Laure Barra,[d] Aloysius G. M. Jansen,[d] Eva Rentschler,[e] and Grigore A. Timco[f]

Abstract: A new tetragonal ($P42_12$) crystalline form of $[Cr_8F_8Piv_{16}]$ (HPiv = pivalic acid, trimethyl acetic acid) is reported. The ring-shaped molecules, which are aligned in a parallel fashion in the unit cell, form almost perfectly planar, regular octagons. The interaction between the Cr^{III} ions is antiferromagnetic ($J = 12\ cm^{-1}$) which results in a $S = 0$ spin ground state. The low-lying spin excited states were investigated by cantilever torque magnetometry (CTM) and high-frequency EPR (HFEPR). The compound shows hard-axis anisotropy. The axial zero-field splitting (ZFS) parameters of the first two spin excited states ($S = 1$ and $S = 2$, respectively) are $D_1 = 1.59(3)\ cm^{-1}$ or $1.63\ cm^{-1}$ (from CTM and HFEPR, respectively) and $D_2 = 0.37\ cm^{-1}$ (from HFEPR). The dipolar contributions to the ZFS of the $S = 1$ and $S = 2$ spin states were calculated with the point dipolar approximation. These contributions proved to be less than the combined single-ion contributions. Angular overlap model calculations that used parameters obtained from the electronic absorption spectrum, showed that the unique axis of the single-ion ZFS is at an angle of $19.3(1)^\circ$ with respect to the ring axis. The excellent agreement between the experimental and the theoretical results show the validity of the used methods for the analysis of the magnetic anisotropy in antiferromagnetic Cr^{III} rings.

Keywords: antiferromagnetic rings · cantilever torque magnetometry · chromium · high-field high-frequency EPR spectroscopy · magnetic anisotropy · molecular magnets

Introduction

Since the discovery that the $[Mn_{12}O_{12}(CH_3COO)_{16}(H_2O)_4]$ molecule shows slow relaxation of the magnetization at low temperatures,[1, 2] intense scientific investigations of this and other single-molecule magnets (SMM) have been performed because they are promising new materials for data storage and quantum computing. Apart from the need for a high-spin ground state, a molecule that is to function as a SMM should have a large negative zero-field splitting (ZFS) to create a barrier for magnetization inversion. Progress in synthetic chemistry has made rational design of high-spin cluster molecules possible and spin ground state values of as large as $S = 51/2$ have been obtained.[3] The other factor, that of ZFS, is less understood at this moment, and concurrently less controllable. Since the discovery of Mn_{12}, many other complexes were synthesized that behave as SMM, for example, $[Mn_4O_3Cl(O_2CCH_3)_3(dbm)_3]$ (Hdbm = dibenzoylmethane),[4] $[Fe_4(OCH_3)_6(dpm)_6]$ (Hdpm = dipivaloylmethane),[5] $[Fe_8O_2(OH)_{12}(tacn)_6]Br_8$ (tacn = 1,4,7-triazacyclononane),[6] and $[V_4O_2(O_2CR)_7(bpy)_2]$ (bpy = 2,2′-bipyridine).[7] However, for all of these complexes, lower temperatures than in the case of Mn_{12} are needed to observe SMM behavior. This means that over the past years no progress has been made towards SMMs that function at higher temperatures. Therefore, it is a necessity to gain an understanding of the origins and to control the magnetic anisotropy to make rational design of SMMs possible.

Antiferromagnetic even-membered rings are characterized by an $S = 0$ ground state, which makes them unsuitable as a

[a] D. Gatteschi, J. van Slageren, R. Sessoli
Dipartimento di Chimica
Università degli Studi di Firenze and UdR, INSTM di Firenze
Via della Lastruccia 3, 50019 Sesto Fiorentino (Italy)
Fax: (+39) 055-4573372
E-mail: dante.gatteschi@unifi.it

[b] A. A. Smith, M. Helliwell, R. E. P. Winpenny
Department of Chemistry, University of Manchester
Oxford Road, Manchester, M13 9PL (UK)

[c] A. Cornia
Dipartimento di Chimica
Università degli Studi di Modena e Reggio Emilia
Via G. Campi 183, 41100 Modena (Italy)

[d] A.-L. Barra, A. G. M. Jansen
Grenoble High Magnetic Field Laboratory
Max-Planck-Institut für Festkörperforschung and Centre National de la Recherche Scientifique
BP 166, 38042 Grenoble, Cedex 9 (France)

[e] E. Rentschler
Max-Planck-Institut für Strahlenchemie
Stiftstrasse 34–36, 45470 Mülheim an der Ruhr (Germany)

[f] G. A. Timco
Academy of Sciences of the Republic of Moldova, Institute of Chemistry
Str. Academiei, 3, 2028 Chişinău (Moldava)

  0947-6539/02/0801-0277 $ 17.50+.50/0

SMM. However, they are interesting because they can serve as model systems for 1-D magnetic materials, as well as show large quantum effects, such as tunneling of the Néel vector.[8–13] Another matter of interest for this kind of system is that they form a very suitable series of complexes to investigate the origins of magnetic anisotropy, partly because of their high symmetry, which is often crystallographically imposed, but sometimes idealized. The magnetic anisotropy can manifest itself not only in the response of the ions in a molecule to an external field (g value anisotropy), but also as a splitting of a spin state manifold in the absence of a magnetic field (zero-field splitting, ZFS). In general, the total magnetic anisotropy of clusters is the sum of several factors:[14] 1) The sum of the single-ion anisotropies of the transition metal ions. This factor is determined by the nature of the ground state of the metal ion and its separation from excited states, by the nature of the ligands, their geometry around the metal center as well as the size of the spin-orbit coupling (SOC) constant. 2) The dipolar interaction between the ions, which depends on the distance between them. 3) The anisotropic exchange interaction between the ions, which relies on the admixture of excited states into the ground state by SOC.[15]

Recently, systematic approaches have been made to rationalize the magnetic anisotropy in antiferromagnetic iron(III) rings. Many different techniques, including high-field EPR spectroscopy, inelastic neutron scattering, torque magnetometry, and diamagnetic dilution were used to show that the observed anisotropy is given by a sum of two terms, namely single-ion anisotropy and dipolar interactions.[16–21] In particular, the interplay between these factors can be very sensitive to slight changes in the coordination geometry around the metal atom. For example, if the cation M in $[MFe_6(OCH_3)_{12}(R\text{-dbm})_6]^+$ is changed from Li^+ to Na^+, then the axial ZFS parameter D_1 of the first excited spin state ($S = 1$) changes from 1.16(1) cm^{-1} to 4.32(3) cm^{-1}. This effect could ultimately be related to a relatively small change in the coordination geometry around the Fe^{III} ions.[17–19] So far, all sophisticated magnetic anisotropy studies have been performed on Fe^{III} rings. Therefore, it would be of interest to analyze in detail the magnetic anisotropy of antiferromagnetic rings of other paramagnetic ions, such as Cr^{III}. This study aims to investigate whether the experimental and theoretical methods and techniques, that were used so successfully in the Fe^{III} rings, are valid for rings of ions that are expected to behave more like quantum spins, for example Cr^{III}. It is necessary to know if these methods are generally applicable in the study of the anisotropy of paramagnetic compounds.

Here we present the synthesis, crystal structure, magnetism and magnetic anisotropy of $[Cr_8F_8Piv_{16}]$ (HPiv = pivalic acid, trimethyl acetic acid) (**1**). A new crystal form of **1** (which is tetragonal, **1t**, in contrast to the previously published monoclinic form, **1m**, vide infra) is reported. Furthermore, the zero-field splittings (ZFS) of the first excited spin states are studied by cantilever torque magnetometry and high-frequency EPR. The total ZFS is separated into single-ion and dipolar contributions by means of point-dipolar and angular overlap model (AOM) calculations.

Results and Discussion

Synthesis: $[Cr_8F_8Piv_{16}]$ (**1**) is the highest nuclearity Cr–F compound known to us. Other Cr–F complexes include the dinuclear and tetranuclear complexes $[Cr_2F_2L_2]$ and $[Cr_4F_4L_4]$ (L is a tetrahydrosalen derivative)[22, 23] and $(NEt_4)_3[Cr_2F_9]$.[24] Complex **1** is one of quite a few ring-shaped first-row transition metal complexes that have been reported the last few years; examples include Cr_8,[25, 26] Cr_{10},[27] Mn_6,[28] Fe_6,[19] Fe_{10},[29] Fe_{12},[30] Fe_{18}[31] and Ni_{12}.[32]

Crystal structure: The crystal structure of **1**, crystallized from acetone, was reported in the literature to be monoclinic ($P2_1/c$) with four molecules in the unit cell.[33, 34] In the following, complex **1** in this crystal form will be denoted **1m**. In contrast, crystallization from hexane reproducibly yields crystals belonging to the tetragonal space group $P42_12$; these crystals will be denoted **1t**. In these crystals, the molecules are aligned in a parallel fashion, and one unit cell contains four halves of molecules. An ORTEP plot of one molecule of **1t** viewed down the c axis of the crystal is shown in Figure 1.

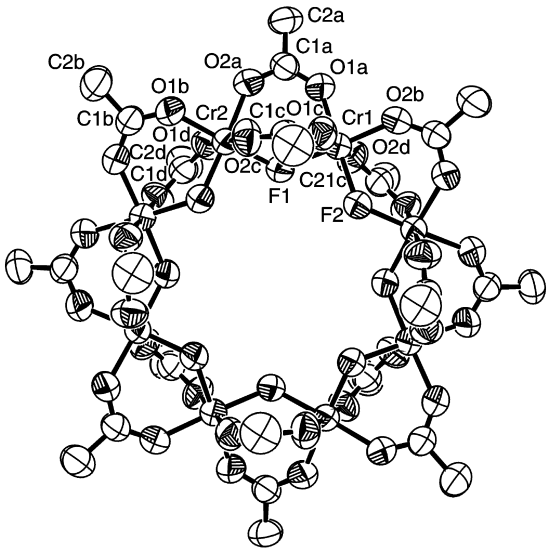

Figure 1. Displacement ellipsoid plot of **1** (50% probability level). The disordered solvent molecule as well as the (disordered) methyl groups have been omitted for clarity. In the case of the disordered C2 atom (see text), one position is shown (C21c).

The asymmetric unit consists of two chromium and fluoride ions, as well as four pivalate groups. The coordination environment of the chromium ions is slightly distorted octahedral. The bond angles around the Cr^{III} ions range from 86.46(17)° to 92.9(2)° (*cis*) and from 177.72(15)° to 179.23(16)° (*trans*). Table 1 lists the most important bond lengths and angles for **1t**. The Cr^{III} ions form an almost perfectly planar octagon (maximum deviation from the least-squares plane through the Cr ions is 0.08 Å). The average nearest neighbor distance, Cr···Cr, is 3.388 ± 0.002 Å. At the molecular level, both crystal forms are very similar: in **1m** the average distances and angles are: Cr···Cr 3.389 ± 0.007 Å, Cr–F 1.916 ± 0.006 Å, Cr–O 1.947 ± 0.007 Å, Cr-F-Cr 124.4 ± 0.2°. The largest difference between **1m** and **1t** is the maximum

0947-6539/02/0801-0278 $ 17.50+.50/0 *Chem. Eur. J.* **2002**, *8*, No. 1

Table 1. Important bond lengths [Å] and angles [°] of non-hydrogen atoms of **1t**. Esd in digit in parentheses.

Bond	length [Å]	Bond	angle [°]
Cr1–F1	1.911(3)	Cr1-F1-Cr2	124.35(14)
Cr1–F2	1.917(3)	Cr2-F2-Cr1[4][a]	124.63(15)
Cr2–F2	1.907(3)	F1-Cr1-F2	89.77(12)
Cr2–F1	1.920(3)	O1a-Cr1-O1c	91.2(2)
Cr1–O1a	1.951(4)	O2b-Cr1-O2d	91.8(2)
Cr1–O1c	1.942(4)	F2-Cr1-O2b	92.19(14)
Cr1–O2b	1.950(4)	F1-Cr1-O2b	177.82(15)
Cr1–O2d	1.947(4)	F2-Cr1-O1a	178.37(14)
Cr2–O1b	1.964(4)	O1c-Cr1-O2d	179.23(16)
Cr2–O1d	1.949(4)	F2-Cr2-F1[4][a]	90.51(12)
Cr2–O2a	1.955(4)	O2a-Cr2-O2c	91.5(2)
Cr2–O2c	1.963(4)	O1b-Cr2-O1d	92.9(2)
		F1-Cr2-O2a	91.87(15)
		F1-Cr2-O1b	177.72(15)
		F2[2]-Cr2-O2a[a]	177.28(14)
		O2c-Cr2-O1d	178.99(17)

[a] Symmetry-equivalent atom, generated by the fourfold axis.

deviation of the Cr^{III} ions from the Cr_8 plane, which is 0.20 Å in the case of **1m**.[33, 34]

Magnetic properties: Preliminary measurements showed that there is a weak antiferromagnetic interaction between the Cr^{III} ions in **1m**.[35] In fact, the χT versus T curves, recorded on polycrystalline powder samples of **1t** and **1m** show a χT value close to zero at low temperatures, and a maximum in χ at 40 K (Figure 2). This indicates a dominating antiferromagnetic

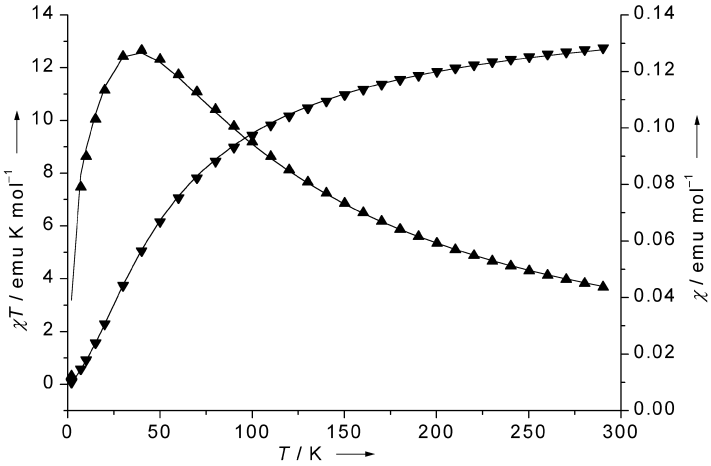

Figure 2. χT (▼) and χ (▲) of **1m** together with the fit (drawn lines) for $g = 1.98$ and $J = 11.9\ cm^{-1}$ (**1m**).

interaction between the Cr^{III} ions and hence an $S = 0$ ground state. At 300 K, the χT value reaches a value of 12.6 emu K mol^{-1} for **1t** (12.7 emu K mol^{-1} for **1m**). The calculated value for eight non-interacting Cr^{III} ions and $g = 1.98$ is slightly higher (14.70 emu K mol^{-1}). Using the effective Heisenberg spin Hamiltonian [Eq. (1)] the experimental data were fit by the Clumag program.

$$H = J\sum_{i=1}^{7} \mathbf{S}_i \cdot \mathbf{S}_{i+1} + JS_8 \cdot S_1 \qquad (1)$$

This program reduces the size of the matrices that describe the magnetic interactions by means of the total spin symmetry of the molecule by irreducible tensor operator techniques, grouping the $(2S+1)^N = 4^8 = 65\,536$ states into matrices with equal total spin.[36] Thus, the largest matrix that has to be calculated is that for $S = 3$ (1505×1505). This procedure yields antiferromagnetic exchange interaction constants J of 12.1 cm^{-1} for **1t** and 11.9 cm^{-1} for **1m** (Figure 2), which fit the experimental data rather well. These J values are comparable to those of other Cr_8 rings, for example $J = 12.0\ cm^{-1}$ for $[Cr_8(OH)_8(O_2CPh)_{16}]$,[26] and $J_1 = 9.5\ cm^{-1}$ and $J_2 = 6.2\ cm^{-1}$ for $[Cr_8(OH)_{12}(O_2CH_3)_{12}]$,[25] as well as to those for four-membered Cr^{III} rings $[Cr_4F_4L_4]$ (L is a tetrahydrosalen derivative)[23] where the nearest-neighbor exchange-interaction parameter is given by $J = 9.7\ cm^{-1}$ and $11.1\ cm^{-1}$ for two different ligands L, respectively. Slightly larger exchange couplings were found for antiferromagnetic Fe_6 rings (12–20 cm^{-1}).[19, 20, 28, 29, 37, 38] A much smaller coupling constant was found for $[Cr_{10}(O_2CMe)_{10}(OEt)_{20}]$ (0.9 cm^{-1}), while for the corresponding OMe complex, even ferromagnetic exchange interaction was found.[27]

Cantilever torque magnetometry (CTM): From the fit of the magnetic susceptibility data, an energy gap between the $S = 0$ ground state and the $S = 1$ first spin excited state (Δ_1) of 6.70 cm^{-1} was found in the absence of a magnetic field. Since in a magnetic field that is applied parallel to the molecular z axis the energy levels vary as $E = M_S \cdot g \cdot \mu_B \cdot H$, the $M_S = -1$ component of the $S = 1$ triplet state is expected to cross the $S = 0$ state at $H = \Delta_1/g \cdot \mu_B = 7.25$ T. A CTM study on a single crystal of **1t** was undertaken to verify this expectation, as well as to derive the anisotropy parameters of the $S = 1$ spin state. Because the molecules are positioned in a parallel fashion in the crystal, which has a tetragonal space group, the crystal anisotropy corresponds to the molecular anisotropy and must be of the unique axis type, where the unique axis is the ring axis. The cantilever can be rotated along one axis, which is perpendicular to the magnetic field. In these studies, the crystal is mounted on the cantilever so that the unique axis is perpendicular to the axis of rotation (Figure 3). The capacitance between the plates can then be measured as a function

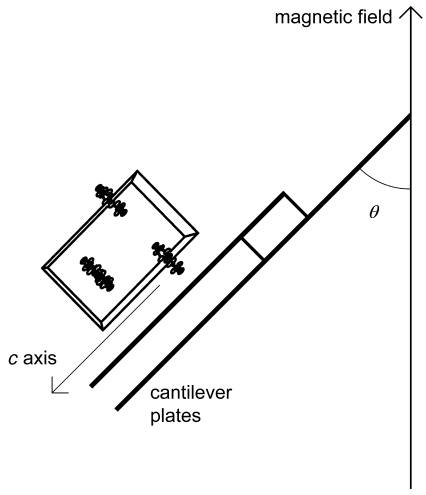

Figure 3. Cantilever setup, showing the direction of the unique axis and the magnetic field.

of magnetic field and of the angle between the unique axis and the field.

Indeed, the torque curve recorded as a function of the magnetic field shows a distinct step at about 7 Tesla, which is rather broad at 4 K, but quite pronounced at 0.4 K (Figure 4). The torque signal for an anisotropic paramagnet with spin S and ZFS parameter D_S saturates to a value proportional to D_S in high fields.[18] Hence, the step points to a nonzero magnetic

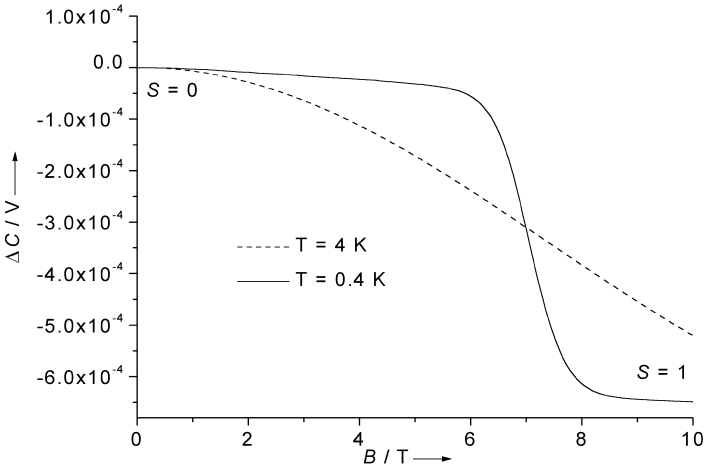

Figure 4. The change in capacitance signal of the oriented single crystal of **1t** as a function of the magnetic field ($\theta_{exp} = 45°$).

anisotropy in the $S = 1$ state as compared to the non-magnetic character of the singlet ground state.[14] Because the capacitance decreases, that is the gap between cantilever plates widens, it is clear that the crystal tends to orient the unique axis perpendicular to the magnetic field going from the $S = 0$ to the $S = 1$ state (Figure 1). Thus, it is clear that the cluster has a hard-axis anisotropy along c.

The expression that describes the dependence of the field at the inflection point as a function of the angle between the unique axis and the applied field (at high magnetic field)[14, 18] simplifies to Equation (2) in this particular case of an $S = 0$ to $S = 1$ transition.

$$B_c = \frac{\Delta_1 + (\cos^2\theta - 1/3) \times 1/2\, D_1}{g\mu_B} \quad (2)$$

In B_c is the critical field at the inflection point in the torque curve, Δ_1 is the separation between the singlet state and the barycenter of the triplet state (at zero field), $\theta = \theta_{exp} + \theta_0$ is the real angle between the unique axis and the applied magnetic field, θ_{exp} is the experimentally determined angle between the unique axis and the magnetic field, θ_0 is the misalignment angle of the crystal, D_1 is the zero-field splitting of the $S = 1$ state and $\mu_B = 0.4669\ cm^{-1}T^{-1}$. Figure 5 shows the plot of B_c versus θ_{exp}, recorded at 0.4 K. The error bars indicate the difference in inflection point between the upfield and downfield sweeps, and show that instrumental hysteresis is negligible. Least-squares fitting of the B_c versus θ_{exp} plot to Equation (2), yields the following parameters: $\Delta_1 = 6.509(8)\ cm^{-1}$, $D_1 = 1.59(3)\ cm^{-1}$, $\theta_0 = -9.6(9)°$. The g value was set to 1.98, which is a common value for Cr^{III}, and confirms to that observed in X-band EPR measurements of

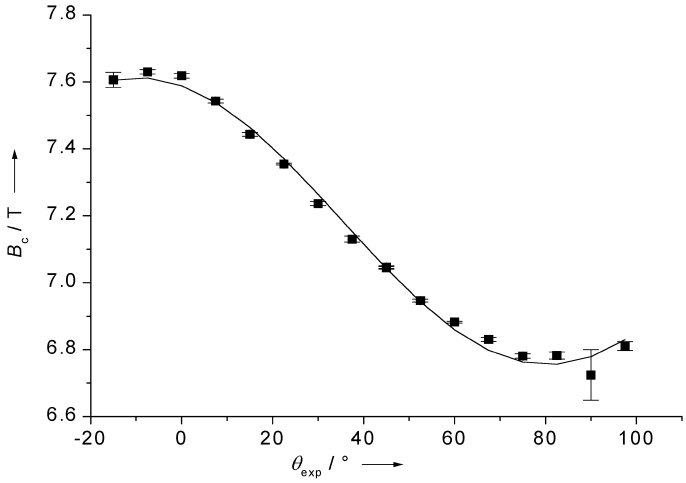

Figure 5. The crossing field as a function of the angle between unique axis and the applied magnetic field ($T = 0.4$ K).

1m,[33, 34] and indeed is obtained from the fit of the HFEPR data (vide infra). The Δ_1 value, obtained from the fit of the B_c versus θ_{exp} plot (6.509(8) cm^{-1}), compares well with that found from the fit of the magnetic susceptibility data (6.70 cm^{-1}).

High-frequency EPR (HFEPR): HFEPR provides another way to obtain the magnetic anisotropy parameters of paramagnetic clusters with an accuracy comparable to CTM.[14, 18] The spectra were recorded on powder samples of **1** at various temperatures (1.6 to 25 K) at 115 and 230 GHz on a pellet of ground powder, in order to prevent orientation effects. The spectra recorded at 230 GHz are shown in Figure 6. The spectra have been truncated at 6 T for reasons of clarity. In addition to the shown lines, one strong line was observed at 4.02 T and is attributed to the $\Delta M_S = 2$ transition. Note that the sharp, intense feature at 8.68 T has been truncated so that the less intense bands are discernible. The 230 GHz frequency

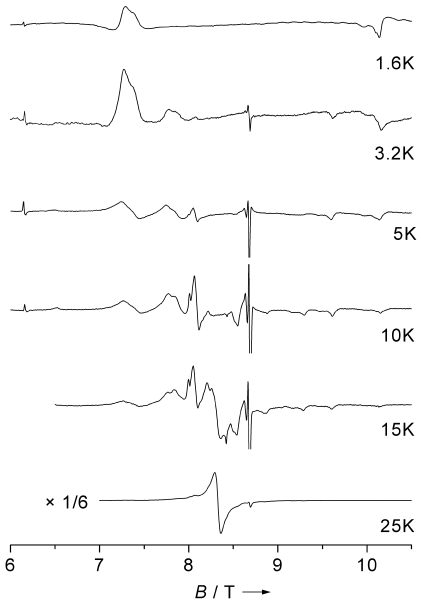

Figure 6. High-frequency (230 GHz) EPR spectra recorded on a powder sample of **1** at various temperatures.

0947-6539/02/0801-0280 $ 17.50+.50/0 *Chem. Eur. J.* **2002**, *8*, No. 1

was obtained by frequency doubling of the 115 GHz fundamental. Because no low-pass filter was employed, the third harmonic (345 GHz) is also present (albeit in low intensity) in the irradiating beam. This gives rise to the signal at 6.15 T in the spectrum (Figure 6). From the temperature dependence of the spectra, it is clear that the spectra consist of varying contributions from the $S=1$ and $S=2$ states. Thus, at 1.6 K only the bands from the $S=1$ state are visible. On warming the sample, signals from $S=2$ appear. At temperatures higher than 15 K, a strong signal at 8.33 T appears. This is attributed to peaks from higher lying excited states.

The spectra were fitted by independently simulating spectra for $S=1$ and $S=2$ at various temperatures, which were then added. Before adding the simulated spectra together, the spectrum for $S=2$ was multiplied by a factor that reflects the magnetic field-dependent Boltzmann population difference between the $S=1$ and $S=2$ states. The best-fit parameters for $S=1$ are $g=1.98$, $D_1=1.63\ \mathrm{cm^{-1}}$, $E_1=0.03\ \mathrm{cm^{-1}}$, and for $S=2$ they are $g=1.98$, $D_2=0.37\ \mathrm{cm^{-1}}$, $E_1=0.009\ \mathrm{cm^{-1}}$. Figure 7 shows the fit at 5 K. These parameters fit both the 115 GHz and 230 GHz spectra as well as the spectra at the various

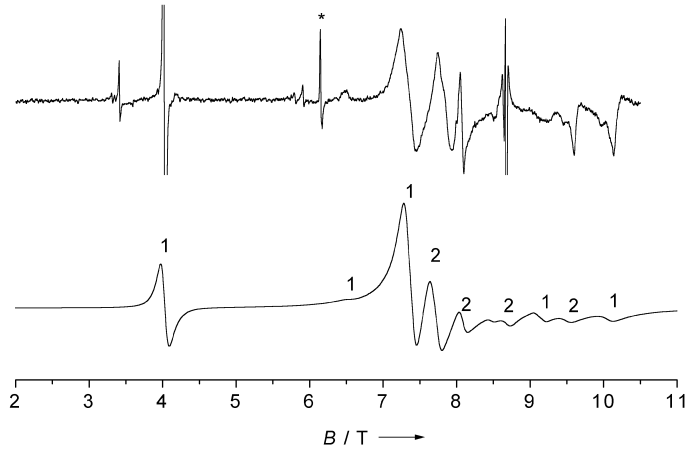

Figure 7. High-frequency (230 GHz) EPR spectrum recorded on a powder sample of **1** at 5 K (top) together with the best obtained fit (bottom): $S=1$: $D_1=1.63\ \mathrm{cm^{-1}}$, $E_1=0.03$; $S=2$: $D_2=0.37\ \mathrm{cm^{-1}}$, $E_2=0.009\ \mathrm{cm^{-1}}$. The numbers 1 and 2 denote signals from the $S=1$ and $S=2$ states, respectively. The asterisk denotes a signal from the 345 GHz third harmonic of the 115 fundamental frequency.

temperatures. Inclusion of a small g value anisotropy did not result in a better fit; whereas inclusion of a small rhombic distortion did, in spite of the fact that rhombic distortion is not expected for a tetragonal system. The explanation of this apparent discrepancy might lie in the fact that the measurements were performed on powdered crystals pressed into a pellet. During this process, the sample has probably lost its lattice solvent which might have resulted in the small distortion observed. Although this fitting procedure does not directly give a standard deviation in the resulting D_1 value, we expect it to be similar to that from the torque measurements. Note that the fit does not reproduce well the sharp, intense features at 4.02 T and 8.68 T (Figure 7).

Many antiferromagnetic rings do not give rise to clear EPR signals. This might be caused by extreme dipolar broadening or fast spin-lattice relaxation effects. To our knowledge, this is only the second example of an antiferromagnetic ring that yields clear EPR spectra, after $[Fe_6(tea)_6]$ (H_3tea = triethanol amine).[37] The D_1 value obtained for **1** from the HFEPR spectra ($1.63\ \mathrm{cm^{-1}}$) corresponds very well to that found from the torque measurements ($1.59(3)\ \mathrm{cm^{-1}}$, vide supra). To our knowledge, this is the first antiferromagnetic Cr^{III} ring for which the ZFS parameters of the excited spin states have been determined. The D_1 value is quite similar to that of $[LiFe_6(OCH_3)_{12}(dbm)_6]PF_6$ ($D_1=1.16(1)\ \mathrm{cm^{-1}}$), while for other antiferromagnetic rings, D_1 values between $0.2\ \mathrm{cm^{-1}}$ ($[NaFe_6(tea)_6]Cl$)[20] and $8.2\ \mathrm{cm^{-1}}$ ($Fe_6(tea)_6$])[37] were found. For Cr^{III} dimers a number of ZFS parameter data exist, for example $[Cr_2(OH)_3(Me_3tacn)_2](ClO_4)_3$ (Me_3tacn = 1,4,7-trimethyl-1,4,7-triazacyclononane), $|D_1|=2.28\ \mathrm{cm^{-1}}$ (from EPR)[39] or $D_1=-2.25(1)\ \mathrm{cm^{-1}}$ (from optical spectroscopy).[40] In other cases, the axial ZFS parameter was found to be negative as well,[41] in contrast to **1** and to other antiferromagnetic rings. This might be peculiar to dimers, since the calculated dipolar contribution to the ZFS in dimers is negative.[41]

Calculations: The system under study may be described by the spin Hamiltonian given in Equation (3).

$$H=\mu_B \boldsymbol{g}\cdot\boldsymbol{B}\cdot\boldsymbol{S}+\boldsymbol{S}\cdot\boldsymbol{D}_S\cdot\boldsymbol{S} \tag{3}$$

Where $\boldsymbol{D}_S$ is the ZFS tensor. As mentioned in the introduction, the ZFS tensor is the combination of the single-ion ZFS tensor and the spin–spin interaction ZFS tensor. The ZFS tensor of the total spin state S, $\boldsymbol{D}_S$, can be expressed by projecting the individual spins on the total spin [Eq. (4)].[15]

$$\boldsymbol{D}_s=\sum_{i=1}^{N} d_i^S \boldsymbol{D}_i+\sum_{i<j}^{N} d_{ij}^S \boldsymbol{D}_{ij} \tag{4}$$

Where N is the number of metal ions in the ring, d_i are the single ion projection coefficients, d_{ij} are the spin–spin interaction coefficients, and $\boldsymbol{D}_i$ and $\boldsymbol{D}_{ij}$ are the single-ion and spin–spin ZFS tensors, respectively. In principle, the spin–spin ZFS tensors include contributions from dipolar and anisotropic exchange terms. An order-of-magnitude estimate for the latter is given by $(\Delta g/g)^2\cdot J\approx 0.01\ \mathrm{cm^{-1}}$ (where Δg is the deviation of the g value from the spin-only value).[15] However, it must be remembered that the use of J in the order-of-magnitude estimation is not correct because theoretically one should use the interaction between one ion in the ground state and the other in the excited state. In fact, large deviations from this behavior were clearly observed in dinuclear copper(II) complexes.[15] Indeed, some authors attribute the spin–spin ZFS contribution in chromium(III) compounds completely to dipolar interactions,[42] while in other cases the dipolar interaction does not account completely for the axial ZFS found.[39, 41] However, in these latter cases, the axial ZFS parameters were of the order of a few hundredths of a wavenumber, which makes the relative error quite large. In the sulfur-centered tetranuclear Cr^{III} complex $[SCr_4(O_2CCH_3)_8(H_2O)_4](BF_4)_2\cdot H_2O$, anisotropic exchange was thought to be present; it caused broadening of the

observed EPR lines.[43] The contribution of the anisotropic exchange to the axial ZFS is assumed to be negligible in the case of **1**.

The d_i and d_{ij} coefficients can be calculated by means of a suitable coupling scheme for the spins. For this it is necessary to know the nature of the ground state. By analogy to the method used in the analysis of the antiferromagnetic iron(III) rings,[19] the octanuclear ring was divided into two squares of next-nearest neighbors which are ferromagnetically coupled to give the states of maximum multiplicity, $S_I = 6$. The two resulting S_I states are then coupled to give $S = 0$. The spin functions can therefore be expressed as $|S_1\, S_3\, S_{13}\, S_5\, S_{135}\, S_7\, S_{1357}\, S_2\, S_4\, S_{24}\, S_6\, S_{246}\, S_8\, S_{2468}\, SM\rangle$. The analysis of the iron(III) rings showed that the lowest lying $|SM\rangle$ levels are well described by the above functions. The behaviour of Cr^{III} that has a spin of 3/2 is closer to that of a quantum spin than Fe^{III}. This could mean that the above functions are not a valid description of the lowest spin states anymore. However, a Clumag calculation, that uses this coupling scheme, showed that the lowest spin states are still quite well ($\approx 70\,\%$) described by the above functions. The calculated coefficients are reported in Table 2. Calculations on spin states with the same total spin but described by other functions gave almost the same ratio of the two d_{ij} coefficients. Hence the results should be quite insensitive to the approximation that we made in the description of the spin states. The $\boldsymbol{D}_{ij}$ tensor was then calculated, in the point dipolar approximation, by summing all the possible interactions (nearest neighbor, next-nearest neighbor and so on), taking into account the angle of the vector between the interacting ions and their distance. This procedure finally resulted in a dipolar contribution to the ZFS parameter of the $S = 1$ state, D_1^{dip}, of 0.490 cm^{-1}. For the $S = 2$ state, the corresponding contribution is lower, namely $D_2^{dip} = 0.122\ cm^{-1}$. If the exchange anisotropy contribution is neglected, then the axial ZFS parameter of spin state S is given by the sum of the dipolar and total single-ion contributions, $D_S = D_S^{dip} + D_S^{si}$. Subtracting the dipolar contribution from the total axial ZFS parameter gives a total single-ion contribution of $D_1^{si} = 1.120\ cm^{-1}$ for $S = 1$ (D_1 was taken as 1.61 cm^{-1}, the average of the values obtained from CTM and HFEPR). Since the single-ion axial anisotropies are projected on the total anisotropy for $S = 1$ with a calculated coefficient d_i of -0.75 (Table 2), the component along the ring axis of the single-ion contribution to the axial ZFS parameter per Cr ion is $d_{zz}^{Cr} = -0.187\ cm^{-1}$. Projecting this d_{zz}^{Cr} value on the $S = 2$ state gives a total single-ion contribution, $D_2^{si} = 0.248\ cm^{-1}$ for $S = 2$. That means that the total axial ZFS parameter for $S = 2$ is $D_2 = 0.248 + 0.122 = 0.370\ cm^{-1}$. This is exactly the same value that was found from the EPR fitting. In view of the excellent agreement of calculated and experimental values, a neglect of the anisotropic exchange part of the spin-spin interaction contribution to the ZFS seems to be justified. All the contributions to the axial ZFS parameters of both the $S = 1$ and $S = 2$ states of **1** are given in Table 2.

Similar calculations were performed for $[LiFe_6(OCH_3)_{12}(dbm)_6]^+$ and $[NaFe_6(OCH_3)_{12}(pmdbm)]^+$ (Hpmdbm = 1,3-di(4-methoxyphenyl)-1,3-1,3-propanedione).[18] These proved that the dipolar contributions to D_1 for the two derivatives are similar to each other (1.24 and 1.15 cm^{-1}, respectively) and to that of **1**, while the total single-ion contribution, D_1^{si} is hugely different (-0.08 and 3.17 cm^{-1}, respectively). This latter result was assumed to originate in a larger twist angle around the Fe^{III} ions for the sodium derivative.

Many Cr^{III} single-ion axial ZFS parameters have been reported in the literature. A large number were derived from measurements of mononuclear complexes,[44, 45] or Cr^{III} doped in inorganic lattices,[46] with absolute values ranging between practically negligible to $\approx 0.7\ cm^{-1}$. For dimeric complexes, typical values range from $|D_{zz}^{Cr}| = 0.198(2)\ cm^{-1}$,[42] to $D_{zz}^{Cr} = -0.658\ cm^{-1}$.[22] The single-ion axial anisotropy found for **1** fits into this range. A method to obtain direct experimental evidence for the single-ion contribution to the ZFS is the replacement of paramagnetic ions in the compound under study by diamagnetic ones. This method was successfully applied for the substitution of Cr^{III} by Co^{III} in Cr^{III} dimers,[47] and also in by doping a six-membered ring Ga^{III} with Fe^{III} in the case of the Fe_6 rings described above.[16]

Angular overlap model (AOM) calculations were used to obtain an indication of the direction and magnitude of the single-ion ZFS of **1**. This model was used to calculate the ZFS parameters from the spin-orbit coupling constant, the Racah B and C parameters as well as parameters that describe the σ and π bonding capabilities of the ligands, e_σ and e_π, respectively.[48, 49] The coordination geometry around Cr was assumed to be non-distorted octahedral. From a combination of the UV/Vis spectra and literature data, reasonable values can be obtained for the mentioned parameters. In a first-order approximation the energy of the spin-forbidden $^4A_{2g} \rightarrow {}^2E_g$ transition (in O_h notation) is given by $9B + 3C$.[49] A typical value for the Racah B parameter in Cr^{III} complexes is 600 cm^{-1}.[49, 50] Since the spin-forbidden quartet–doublet transition is observed for **1** at 14728 cm^{-1} in hexane, this yields a value of $\approx 3000\ cm^{-1}$ for C. The symmetry of the coordination around the chromium atoms in **1** is actually C_{2v} and not O_h. It can be shown that the $^4A_{2g}$ ground state in O_h symmetry becomes $^4B_1$ in *cis*-$[MX_4Y_2]$ complexes with C_{2v} symmetry. The lowest quartet level ($^4T_{2g}$ in O_h) splits up into $^4B_2$ and ^4E.[51] The relative position of the latter two levels depends on the relative Dq values of the X and Y ligands. In the present case $Dq(O_2CR^-)$ is expected to be larger than $Dq(F^-)$.[50] This means that ^4E should be higher in energy than $^4B_2$.[51] In the UV/Vis spectrum, a band is observed at $\lambda = 16474\ cm^{-1}$ which has two shoulders at 15337 and 15625 cm^{-1}. The band is attributed to the $^4B_1 \rightarrow {}^4E$ transition, while the

Table 2. Calculated single-ion and dipolar interaction coefficients (d_i and d_{ij} respectively) for **1**.

Spin state	d_i	$d_{i,i+1} = d_{i,i+3}$	$d_{i,i+2} = d_{i,i+4}$	D_S^{dip} [cm^{-1}]	D_S^{si} [cm^{-1}][a]	D_S^{tot} (calcd) [cm^{-1}]	D_S^{tot} (obs) [cm^{-1}]
$S = 1$	-0.750	-1.125	1.063	0.490	1.120	1.61[b]	1.61
$S = 2$	-0.166	-0.248	0.259	0.122	0.248	0.370	0.37

[a] The component along the ring axis of the single-ion contribution per Cr ion, $d_{zz}^{Cr} = -0.187\ cm^{-1}$. [b] Used to calculate D_1^{Cr}, see text.

0947-6539/02/0801-0282 $ 17.50+.50/0 *Chem. Eur. J.* **2002**, *8*, No. 1

two shoulders are attributed to the transition to the $^4B_2$ energy level. For a *cis*-$[MX_4Y_2]$ complex, the energies of those two transitions are given by $\Delta E(^4B_1 \rightarrow {}^4B_2) = 5\,Dq(X) + 5\,Dq(Y)$ and $\Delta E(^4B_1 \rightarrow {}^4B_2) = 15/2\,Dq(X) + 5/2\,Dq(Y)$.[51] In **1**, X = $O_2C(CH_3)_3^-$ and Y = F^-, leading to $Dq(O_2CR^-) = 1745\ cm^{-1}$ and $Dq(F^-) = 1355\ cm^{-1}$. This $Dq(F^-)$ value is slightly lower than the typical value of 1500–1700 cm^{-1}.[49, 50] The spin-orbit coupling constant of the free Cr^{III} ion is $\zeta = 276\ cm^{-1}$,[46] which is expected to be smaller in actual complexes. In this study, 0.8 was used as a reduction factor since this yielded acceptable values for g (1.97) in the resulting fit. For the F^- and $^-O_2C(CH_3)_3$ ligands, values of 0.46 and 0.50 were used for the $2e_\pi/e_\sigma$ ratio; these are typical values obtained from literature.[49, 50] Inserting the above parameters in the program, first of all resulted in calculated spin-forbidden transitions at $\approx$14000 cm^{-1}, and two spin-allowed transitions at 15500 and 16330 cm^{-1}. This is in good agreement with the observed values of 14728, $\approx$15500 and 16474 cm^{-1}, respectively. With these parameters, a total single-ion axial ZFS for one Cr ion of $D^{Cr} = -0.06\ cm^{-1}$ was calculated. Furthermore, the calculations showed that the principal direction of the single-ion ZFS is the O-Cr-O axis, which is at an angle of 19.3(1)° with respect to the ring axis. This means that the single-ion ***D*** tensors are not co-linear with the unique molecular axis, but deviate much less than in the case of $[NaFe_6(OCH_3)_{12}(pmdbm)_6]ClO_4$, where this angle is 79.2(4)°.[16] The component of D^{Cr} along the ring axis is given by $D^{Cr}(ZZ) = D^{Cr}(\cos^2\beta - 1/3)$, neglecting rhombic ZFS, where β is the angle between the principal direction of the ZFS and the ring axis. Hence, from the effective single-ion axial ZFS per Cr atom ($-0.187\ cm^{-1}$, vide supra), the real single-ion axial ZFS per Cr atom is calculated to be $-0.334\ cm^{-1}$, or more than five times the value found from the AOM calculations.

While the AOM model is too simple to predict the magnitude of the single-ion ZFS correctly, it does yield its direction. It was shown that the direction of the single-ion ZFS tensor is of the utmost importance: it was recently demonstrated that the two magnetization relaxation mechanism processes in Mn_{12}Ac are caused by molecules with differently aligned ZFS axes.[52] This means that from this relatively simple model, an estimate of the single-ion contribution to the ZFS can be obtained from the UV/Vis spectral data and literature parameters. This is in contrast to the case of the Fe^{III}, where the UV/Vis spectra are much less informative.

Conclusion

Both cantilever torque magnetometry and high-frequency EPR (HFEPR) are excellent tools to study the magnetic anisotropy of the spin excited states of antiferromagnetic rings. In general, they yield results with comparable accuracy. In this study, the results obtained from both techniques agreed perfectly. The HFEPR results indicate that accurate zero-field splitting (ZFS) parameters of the spin excited states of antiferromagnetic rings may be obtained by using powder samples, and that single crystals are not necessary.

By performing calculations in the point-dipolar approximation, the observed zero-field splittings may be separated into single-ion and dipolar interaction contributions. It was shown that both play a significant role in determining the magnetic anisotropy of **1**, while anisotropic exchange certainly plays a minor role.

Moreover, the combination of UV/Vis spectral and X-ray crystallographic data with AOM and point dipolar calculations can provide an estimate of the axial ZFS of the lowest excited spin states. This is a very important result, since it allows the screening of compounds before embarking on extensive physical studies.

Finally, this study shows that the experimental and theoretical methods used successfully for the Fe^{III} rings are also excellently suited to the study of the magnetic anisotropy in rings of ions with more quantum spin behaviour, such as Cr^{III}.

Experimental Section

Synthesis: The complex $[Cr_8F_8Piv_{16}]$ (**1**) was prepared according to a slightly modified literature procedure.[33, 34] $CrF_3 \cdot 4H_2O$ (Aldrich, 97%; 5.0 g, 28 mmol) and $HO_2CC(CH_3)_3$ (HPiv, Acros, 99%; 11.3 g, 111 mmol) were dissolved in DMF (Acros, 10 mL) and heated with stirring to 140 °C for 4 h. The product was extracted with hexane (50 mL) and separated on a silica gel column using toluene as the eluent. The first fraction from the column was collected and the solution was evaporated to dryness. The final product was crystallised from hexane. Yield: 32% as a green crystalline solid. Elemental analysis calcd (%) for $C_{80}H_{144}O_{32}Cr_8F_8 \cdot C_6H_{14}$: C 45.46, H 7.01, F 6.69; found C 44.85, H 7.18, F 6.21%; UV/Vis (hexane): E = 14728, 15337 sh, 15625 sh, 16474, 23474 cm^{-1}.

Single-crystal structure determination of 1t: Suitable crystals of **1t** were grown by slow evaporation of a hexane solution of **1**. Crystal data: $C_{80}H_{144}O_{32}Cr_8F_8 \cdot 0.25\,C_6H_{14}$, green plate, $0.4 \times 0.3 \times 0.08\ mm^3$, tetragonal, $P42_12$ (no. 90), $a = b = 20.09(2)$ Å, $c = 16.80(2)$ Å, $V = 6782(7)$ Å^3, $Z = 2$, $\rho = 1.079\ g\,cm^{-1}$. The data were collected with a Rigaku RAXIS diffractometer, with a rotating anode ($Mo_{K\alpha}$, $\lambda = 0.71069$ Å) in 94 × 3 degree ϕ oscillations of 30 minutes per exposure at ambient temperature and then processed with the DENZO software.[53] The structure was solved by direct methods with SHELXS 86.[54] 102178 measured reflections, of which 5889 were unique ($R_{int} = 0.066$). The structure was refined with SHELXL 97[55] against F^2 for all reflections with 283 parameters and 48 restraints. The asymmetric unit consists of 1/4 of the molecule, the remainder is generated by operation of the fourfold rotation axis. In addition, a solvent fragment lies on the fourfold axis. This was assumed to be disordered hexane, and therefore, the atoms were defined as carbon and assigned occupancies of 0.5. The *t*Bu groups were highly disordered: in each case, two sites were found for each Me group, whose occupancies were constrained to a sum of 1.0. In the case of one pivalate group, two sites were also found for the C2 atom. Restraints on the bond lengths and angles were also necessary. The ordered non-hydrogen atoms were refined anisotropically, whilst the disordered atoms were refined isotropically. H atoms were included in calculated positions. $R(I > 2\sigma(I))$: $R1 = 0.0679$, $wR2 = 0.1842$. R(all data): $R1 = 0.0848$, $wR2 = 0.2015$.

Crystallographic data (excluding structure factors) for the structure in this paper have been deposited with the Cambridge Crystallographic Data Centre as supplementary publication no. CCDC-164814. Copies of the data can be obtained, free of charge, on application to CCDC, 12 Union Road, Cambridge CB2 1EZ, UK (fax: (+44) 1223-336033 or e-mail: deposit@ccdc.cam.ac.uk).

Physical measurements: The UV/Vis absorption spectrum was recorded on a Perkin-Elmer Lambda 9 spectrophotometer. Magnetic susceptibilities and magnetizations were measured on a Cryogenics S600 SQUID magnetometer. The data were corrected for the diamagnetic contribution using Pascal's constants. Cantilever torque measurements were performed in Grenoble with a CuBe cantilever (∅ upper plate $\approx$2 mm) mounted in a ^{3}He cryostat in an Oxford Instruments 10 T superconducting magnet. The

sample was rotated in the plane defined by the magnetic field and the unique axis. The variation in capacitance, which was assumed to be linearly dependent on the deflection between the plates, was measured with a General Radio 1616 precision capacitance bridge, in combination with a Stanford Research SR830 DSP lock-in amplifier. The field strength was manually swept at $\approx 90\ G\,s^{-1}$ while recording the signal with home-written software. The temperature was monitored with a calibrated RuO_2 resistor. The setup has been described in the literature and is depicted in Figure 3.[16–18, 56]

On account of the complex morphology of the crystals, indexing the faces proved to be an unsuitable method to find the unique axis. Instead, a crystal of **1t** was mounted on a goniometer head and the unit cell was determined on a diffractometer. The direction of the unique axis was indicated by a small piece of glass fibre glued to the crystal mounting fiber. The mounting fiber was then cut and the crystal was put on the top plate of the cantilever under an optical microscope and covered with silicone grease, with the unique axis perpendicular to the axis of rotation and in the plane of the cantilever plates (Figure 3). The positions of the *a* and *b* axes were not determined. Transverse anisotropy could be present, albeit only in fourth order, since the crystal space group is tetragonal. However, fourth order transverse anisotropy was shown to have little influence on CTM measurements.[56]

High-frequency EPR (HFEPR) measurements were performed in Grenoble with a previously described single-pass transmission setup, that consisted of an Oxford Instruments 12 T superconducting magnet, a 115 GHz Gunn diode, with frequency doubler and high pass filter as the excitation source, and a He-cooled InSb bolometer as the detector.[57, 58] The signal from the detector was passed through a lock-in amplifier. Data acquisition and magnet sweeping (typically $50-100\ G\,s^{-1}$) were controlled by home-written software. The powder sample was pressed in order to prevent orientation of the crystallites in the magnetic field. The spectra were fitted using H. Weihe's SIM program.[47, 59]

Acknowledgements

The authors gratefully thank the Laboratoire de Crystallographie of the CNRS in Grenoble for allowing us access to one of their diffractometers. This work was supported by the European Union through the Research Training Network "Molecules as NanoMagnets" under contract number HPRN-CT-1999-00012 and through the Human Potential Programme under contract number HPRI-1999-CT00030. Financial support by the Italian CNR and MURST is gratefully acknowledged.

[1] D. Gatteschi, A. Caneschi, L. Pardi, R. Sessoli, *Science* **1994**, *265*, 1054 – 1058.
[2] R. Sessoli, D. Gatteschi, A. Caneschi, M. A. Novak, *Nature* **1993**, *365*, 141 – 143.
[3] J. Larionova, M. Gross, M. Pilkington, H. Andres, H. Stoeckli-Evans, H. U. Güdel, S. Decurtins, *Angew. Chem.* **2000**, *112*, 1667 – 1672; *Angew. Chem. Int. Ed.* **2000**, *39*, 1605 – 1609.
[4] S. M. J. Aubin, M. W. Wemple, D. M. Adams, H.-L. Tsai, G. Christou, D. N. Hendrickson, *J. Am. Chem. Soc.* **1996**, *118*, 7746 – 7754.
[5] A.-L. Barra, A. Caneschi, A. Cornia, F. Fabrizi de Biani, D. Gatteschi, C. Sangregorio, R. Sessoli, L. Sorace, *J. Am. Chem. Soc.* **1999**, *121*, 5302 – 5310.
[6] A.-L. Barra, P. Debrunner, D. Gatteschi, C. E. Schulz, R. Sessoli, *Europhys. Lett.* **1996**, *35*, 133 – 138.
[7] S. L. Castro, Z. Sun, C. M. Grant, J. C. Bollinger, D. N. Hendrickson, G. Christou, *J. Am. Chem. Soc.* **1998**, *120*, 2365 – 2375.
[8] A. Caneschi, D. Gatteschi, C. Sangregorio, R. Sessoli, L. Sorace, A. Cornia, M. A. Novak, C. Paulsen, W. Wernsdorfer, *J. Magn. Magn. Mater.* **1999**, *200*, 182 – 201.
[9] A. Chiolero, D. Loss, *Phys. Rev. Lett.* **1998**, *80*, 169 – 172.
[10] A. Cornia, A. Fort, M. G. Pini, A. Rettori, *Europhys. Lett.* **2000**, *50*, 88 – 93.
[11] A. Lascialfari, D. Gatteschi, F. Borsa, A. Cornia, *Phys. Rev. B* **1997**, *55*, 14341 – 14349.
[12] M.-H. Julien, Z. H. Jang, F. Borsa, M. Horvatić, A. Caneschi, D. Gatteschi, *Phys. Rev. Lett.* **1999**, *83*, 227 – 230.
[13] A. Lascialfari, D. Gatteschi, A. Cornia, U. Balucani, M. G. Pini, A. Rettori, *Phys. Rev. B* **1998**, *57*, 1115 – 1123.
[14] A. Cornia, D. Gatteschi, R. Sessoli, *Coord. Chem. Rev.* **2001**, *219 – 221*, 573 – 604.
[15] A. Bencini, D. Gatteschi, *EPR of exchange coupled systems*, Springer, Berlin, **1990**.
[16] G. L. Abbati, L.-C. Brunel, H. Casalta, A. Cornia, A. C. Fabretti, D. Gatteschi, A. K. Hassan, A. G. M. Jansen, A. L. Maniero, L. Pardi, C. Paulsen, U. Segre, *Chem. Eur. J.* **2001**, *7*, 1796 – 1807.
[17] A. Cornia, A. G. M. Jansen, M. Affronte, *Phys. Rev. B* **1999**, *60*, 12177 – 12183.
[18] A. Cornia, M. Affronte, A. G. M. Jansen, G. L. Abbati, D. Gatteschi, *Angew. Chem.* **1999**, *111*, 2409 – 2411; *Angew. Chem. Int. Ed.* **1999**, *38*, 2264 – 2266.
[19] A. Caneschi, A. Cornia, A. C. Fabretti, S. Foner, D. Gatteschi, R. Grandi, L. Schenetti, *Chem. Eur. J.* **1996**, *2*, 1379 – 1387.
[20] O. Waldmann, J. Schülein, R. Koch, P. Müller, I. Bernt, R. W. Saalfrank, H. P. Andres, H. U. Güdel, P. Allenspach, *Inorg. Chem.* **1999**, *38*, 5879 – 5886.
[21] O. Waldmann, R. Koch, S. Schromm, J. Schülein, P. Müller, I. Bernt, R. W. Saalfrank, F. Hampel, E. Balthes, *Inorg. Chem.* **2001**, *40*, 2986 – 2995.
[22] R. Sanzenbacher, A. Böttcher, H. Elias, M. Hüber, W. Haase, J. Glerup, T. B. Jensen, M. Neuburger, M. Zehnder, J. Springborg, C. E. Olsen, *Inorg. Chem.* **1996**, *35*, 7493 – 7499.
[23] A. Böttcher, H. Elias, J. Glerup, M. Neuburger, C. E. Olsen, H. Paulus, J. Springborg, M. Zehnder, *Acta Chem. Scand.* **1994**, *48*, 967 – 980.
[24] R. Schenker, S. Heer, H. U. Güdel, H. Weihe, *Inorg. Chem.* **2001**, *40*, 1482 – 1488.
[25] M. Eshel, A. Bino, I. Felner, D. C. Johnston, M. Luban, L. L. Miller, *Inorg. Chem.* **2000**, *39*, 1376 – 1380.
[26] I. M. Atkinson, C. Benelli, M. Murrie, S. Parsons, R. E. P. Winpenny, *Chem. Commun.* **1999**, 285 – 286.
[27] E. J. L. McInnes, C. Anson, A. K. Powell, A. J. Thomson, S. Poussereau, R. Sessoli, *Chem. Commun.* **2001**, 89 – 90.
[28] G. L. Abbati, A. Cornia, A. C. Fabretti, A. Caneschi, D. Gatteschi, *Inorg. Chem.* **1998**, *37*, 1430 – 1431.
[29] G. L. Abbati, A. Cornia, A. C. Fabretti, W. Malavasi, L. Schenetti, A. Caneschi, D. Gatteschi, *Inorg. Chem.* **1997**, *36*, 6443 – 6446.
[30] A. Caneschi, A. Cornia, A. C. Fabretti, D. Gatteschi, *Angew. Chem.* **1999**, *111*, 1372 – 1374; *Angew. Chem. Int. Ed.* **1999**, *38*, 1295 – 1296.
[31] S. P. Watton, P. Fuhrmann, L. E. Pence, A. Caneschi, A. Cornia, G. L. Abbati, S. J. Lippard, *Angew. Chem.* **1997**, *109*, 2917 – 2919; *Angew. Chem. Int. Ed. Engl.* **1997**, *36*, 2774 – 2776.
[32] A. J. Blake, C. M. Grant, S. Parsons, J. M. Rawson, R. E. P. Winpenny, *J. Chem. Soc. Chem. Commun.* **1994**, 2363 – 2364.
[33] N. V. Gérbéléu, Y. T. Struchkov, G. A. Timko, A. S. Batsanov, K. M. Indrichan, G. A. Popovic, *Dokl. Chem.* **1991**, *313*, 232 – 234.
[34] N. V. Gérbéléu, Y. T. Struchkov, G. A. Timko, A. S. Batsanov, K. M. Indrichan, G. A. Popovic, *Dokl. Akad. Nauk SSSR* **1991**, *313*, 1459 – 1462.
[35] E. Rentschler, G. A. Timko, N. V. Gérbéléu, *Proc. 37th IUPAC*, Berlin, **1999**.
[36] D. Gatteschi, L. Pardi, *Gazz. Chim. Italiana* **1993**, *123*, 231 – 240.
[37] B. Pilawa, R. Desquiotz, M. T. Kelemen, M. Weickenmeier, A. Geisselman, *J. Magn. Magn. Mater.* **1997**, *177 – 181*, 748 – 749.
[38] A. Caneschi, A. Cornia, S. J. Lippard, *Angew. Chem.* **1995**, *107*, 511 – 512; *Angew. Chem. Int. Ed. Engl.* **1995**, *34*, 467 – 469.
[39] S. Kremer, *Inorg. Chem.* **1985**, *24*, 887 – 890.
[40] H. Riesen, H. U. Güdel, *Mol. Phys.* **1987**, *1987*, 1221 – 1244.
[41] J. Glerup, H. Weihe, *Inorg. Chem.* **1997**, *36*, 2816 – 2819.
[42] D. Burdinski, E. Bill, F. Birkelbach, K. Wieghardt, P. Chaudhuri, *Inorg. Chem.* **2001**, *40*, 1160 – 1166.
[43] P. K. Kahol, B. J. McCormick, *Chem. Phys. Lett.* **1991**, *184*, 289 – 293.
[44] B. R. McGarvey, *J. Chem. Phys.* **1964**, *41*, 3743 – 3758.
[45] E. Pedersen, H. Toftlund, *Inorg. Chem.* **1974**, *13*, 1603 – 1612.
[46] A. Abragam, B. Bleany, *Electron Paramagnetic Resonance of Transition Ions*, Dover Publications, Inc., New York (USA), **1986**.
[47] J. Glerup, H. Weihe, *Acta Chem. Scand.* **1991**, *45*, 444 – 448.
[48] A. Bencini, I. Ciofini, M. G. Uytterhoeven, *Inorg. Chim. Acta* **1998**, *274*, 90 – 101.

  0947-6539/02/0801-0284 $ 17.50+.50/0

[49] A. B. P. Lever, *Inorganic Electronic Spectroscopy*, Elsevier, Amsterdam, The Netherlands, **1984**.
[50] T. J. Barton, R. C. Slade, *J. Chem. Soc. Dalton Trans.* **1975**, 650–661.
[51] R. Krishnamurthy, W. B. Schaap, J. R. Perumareddi, *Inorg. Chem.* **1967**, *6*, 1338–1352.
[52] S. M. J. Aubin, Z. Sun, H. J. Eppley, E. M. Rumberger, I. A. Guzei, K. Folting, P. K. Gantzel, A. L. Rheingold, G. Christou, D. N. Hendrickson, *Inorg. Chem.* **2001**, *41*, 2127–2146.
[53] Z. Otwinowski, DENZO, A program for automatic evaluation of film densities, New Haven, CT (USA), **1988**.
[54] G. M. Sheldrick, SHELXS-86, a program for the solution of crystal structures, Göttingen (Germany), **1986**.
[55] G. M. Sheldrick, SHELXL-97, a program for crystal structure refinement, Göttingen (Germany), **1997**.
[56] A. Cornia, M. Affronte, A. G. M. Jansen, D. Gatteschi, A. Caneschi, R. Sessoli, *Chem. Phys. Lett.* **2000**, *322*, 477–482.
[57] F. Muller, M. A. Hopkins, N. Coron, M. Grynberg, L. C. Brunel, G. Martinez, *Rev. Sci. Instrum.* **1989**, *60*, 3681–3684.
[58] A. L. Barra, L. C. Brunel, J. B. Robert, *Chem. Phys. Lett.* **1990**, *165*, 107–109.
[59] C. J. H. Jacobsen, E. Pedersen, J. Villadsen, H. Weihe, *Inorg. Chem.* **1993**, *32*, 1216–1221.

Received: June 25, 2001 [F3366]